ACS APPLIED POLYMER MATERIALS

pubs.acs.org/acsapm

Article

Singling Out the Role of Molecular Weight in the Crystallization Kinetics of Polyester/Clay Bionanocomposites Obtained by In Situ Step Growth Polycondensation

Donata I. M. Catalano, Lucia Conzatti, Mohamed Ilsouk, Mohamed Lahcini, Antonella Manariti, Elena Maurina, Mustapha Raihane, Benaissa Rhouta, and Valter Castelvetro*

Cite This: *ACS Appl. Polym. Mater.* 2021, 3, 5405−5415

Read Online

ACCESS | Metrics & More | Article Recommendations | Supporting Information

ABSTRACT: The isothermal crystallization kinetics of a set of bio-nanocomposites produced by in situ catalytic step growth polycondensation of adipic acid and 1,4-butanediol in the presence of Moroccan clay beidellite (BDT) organo-modified with hexadecyltrimethylammonium bromide (cetyltrimethylammonium bromide, CTA) was investigated and compared with that of the parent poly(butylene adipate) (PBA) matrices from which the clay had been extracted. In situ bio-nanocomposites had different contents (0−5 wt %) of CTA/BDT nanofillers characterized by different extents of organo-modification (CTA/BDT equivalent ratios from 0 to 5). The isothermal crystallization rates of the bio-nanocomposites and of the parent PBA matrices were investigated by differential scanning calorimetry (DSC) at 45, 40, and 37 °C and analyzed according to the Avrami model. The bionanocomposites with an intermediate (2 wt %) concentration of organoclays with a higher CTA/BDT ratio (3 and 5) showed the highest exfoliation degree, along with an increase in the crystallization rates, compared to those of the parent PBA matrices, which was larger than that in the other nanocomposites. The lack of a simple correlation between the nanoclay content/composition and crystallization kinetics was ascribed to the molecular mass, an additional variable for in situ bio-nanocomposites as compared to nanocomposites prepared by simple physical blending of nanoclays with a single polymer matrix. The specific contribution of the molecular mass to the crystallization kinetics was untangled from those of the organoclay content and CTA/BDT ratio by comparing each bio-nanocomposite with its parent polymer matrix. The crystallization rate of the nanocomposites was always found to reach a maximum within an intermediate range of molecular weights of the polymer matrix, a behavior previously reported only for pure polymers. Such differences in the crystallization rate of in situ bio-nanocomposites may affect the crystalline phase morphology and, in polymorphs such as in PBA, phase composition, with consequent effects on properties that may be of interest for specific applications.

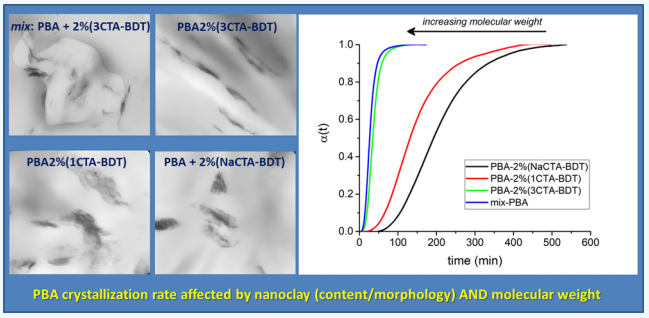

KEYWORDS: *poly(butylene adipate), beidellite nanoclay, in situ polymerization, Avrami model, thermal properties*

Downloaded via UNIV DI PISA on November 12, 2021 at 10:58:15 (UTC).
See https://pubs.acs.org/sharingguidelines for options on how to legitimately share published articles.

1. INTRODUCTION

Aliphatic polyesters are a very interesting class of semicrystalline polymers because of their adjustable thermal mechanical properties, good biocompatibility, and biodegradability.[1,2] The crystallization kinetics of semicrystalline biodegradable materials such as, for instance, poly(butylene adipate) (PBA),[3−5] poly (L-lactide),[6] poly(butylene succinate),[7] and poly(butylene succinate-*co*-adipate)[8] has been extensively investigated. PBA is a polymorph with two main crystalline forms, α and β, the α form being thermodynamically stable at $T > 31$ °C, and the β form at $T < 27$ °C. The enzymatic degradation rate of the α form decreases with increasing crystallinity, with the mixed α/β phase obtained by isothermal crystallization at 28 °C < T < 32 °C showing the lowest biodegradation rate.[3] Because of its low stiffness, slow crystallization rate, low melting point, and modest mechanical properties, pure PBA does not match the requirements for most practical applications.[9] While the physical properties of polyesters may be improved by post-synthetic modifications during, for example, reactive melt processing,[10] PBA is a potentially interesting candidate as a matrix in reinforced biodegradable (nano)composites. In nanocomposites obtained by blending the polymer matrix with natural clays, either as such or as organo-modified

Received: June 7, 2021
Accepted: September 27, 2021
Published: October 6, 2021

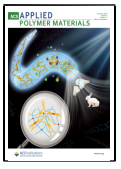

© 2021 The Authors. Published by American Chemical Society

(nano)fillers, the quality of the dispersion affects the ultimate mechanical, thermal, and film barrier properties of the resulting (nano)composite, also referred to as bio-nanocomposite when the polymer matrix is either biodegradable or sourced from renewable materials.[11,12] Relatively small amounts (5 wt % or less) of clays are generally required to optimize the polymer properties, as a result of nanoscale dispersion achieved upon lamellar intercalation with the polymer matrix and/or delamination of the constituting aluminosilicate layers.[13] Beidellite (BDT), a natural layered silicate extracted in the Agadir basin in Morocco,[14] was found to upgrade several features of the polymeric matrix when incorporated into aliphatic polyesters, for instance, poly(ε-caprolactone)[15] and poly(butylene succinate).[16,17] However, the crystalline structure and morphology as well as the crystallization kinetics, all of which affect the ultimate properties of the nanocomposite, may depend not only on the polymer type, the nanoclay content, and the quality of its dispersion (affected, among others, by organophilic nanoclay modifications and, last but not least, by the preparation method[18]) but also on the polymer molar mass.

Along with the common routes to the preparation of nanocomposites by physical blending in solution or in the melt, the in situ polymerization of the monomer(s) in the presence of organo-modified nanoclays represents a soft approach in which monomer/oligomer penetration into, and polymerization within the gallery space, may result in effective nanoclay dispersion and improved properties of the final nanocomposite material.[19] On the other hand, the organoclay may affect the mechanism and kinetics of in situ polymerization, and thus the ultimate polymer molar mass. Indeed, the molar mass of biopolyesters synthesized by step growth polycondensation or ring-opening polymerization in the presence of nanoclays[20] and other nanoparticles (e.g., SiO_2, TiO_2, and layered double hydroxides) has been reported to be generally lower than that of the pure polymer synthesized under the same conditions.[20−23] In the case of purely inorganic nanoparticles, the variation of the molar mass has been attributed to reactions taking place between the nanoparticle's surface functional groups and the reactive end groups of the macromolecule (e.g., polyester[21]). A similar effect observed upon the in situ synthesis of poly(ethylene terephthalate) (PET) in the presence of an organo-modified montmorillonite[20] has also been ascribed to some ill-defined interference of an organic nanoclay modifier with reactive chain ends during polycondensation; on the other hand, an opposite correlation (higher molar mass at a higher nanofiller content) has been reported as well.[24,25] As the molar mass is an important factor affecting the crystallization kinetics of polymer melts and the final semicrystalline morphology, a better understanding of how the molar mass may be affected by the overall content and surface chemical composition of the (organo-modified) nanoclay upon in situ polymer synthesis is of critical relevance to control the nanocomposite properties.

For a pure polymer, the isothermal crystallization rate is known to generally increase with increasing molar mass, reaching a maximum at about 15,000−20,000 g/mole and eventually decreasing at much higher molar masses.[26] Chae et al. studied the crystallization kinetics of linear and branched PBA samples with molar masses ranging from 46,300 to 331,200 g/mol.[5] Within this range, the crystallization rate of both linear and branched PBA samples was found to decrease with increasing molecular weight (with parallel increase in the induction time before nucleation), which is in agreement with the expected behavior in the high molar mass range. In apparent contrast with the general behavior, the crystallization rate of poly(ethylene adipate) with a molecular weight of 10,000 g/mole was found to be lower than that of an oligomeric sample with a molecular weight of 1000 g/mole,[27] suggesting that at a very low molar mass, the crystallization rate increases again as a result of liquid-like molecular mobility.

The crystallization rate of nanocomposites is generally higher than that of the pure polymer matrix with the same (or very similar) molar mass. Several studies concerning nanocomposites containing high aspect ratio nanofillers (e.g., nanoclays) found that such an increase leads to a maximum rate before reversing to lower rates at a higher content of the nanofiller.[3,4,28−31] The important role of the nanoparticles' dispersion state on nucleation and growth, including the effects on the crystalline morphology and the related bulk properties in the final nanocomposite, have also been thoroughly investigated.[32,33] However, when the molar mass is also a variable, a much more complex situation may arise because of the combined effects of the molar mass, nanoclay loading, and extent of the clay organo-modification, when applicable.[22,31] The latter affects the extent of intercalation/delamination/exfoliation of the silicate layers within the polymer matrix, which in turn may significantly affect the crystallization behavior along with several ultimate properties (mechanical, thermal, gas barrier, etc.) of the material. The disaggregation of the original clay particles into tactoids (stacks of single layers) or delamination/exfoliation down to single isolated lamellae may not only increase enormously the concentration of heterogeneities possibly acting as nucleating centers, but also generate physical obstacles to crystal growth propagation. Such nanoclay disaggregation is promoted not only by shear forces (increasing with the increase in molecular mass during polymerization under stationary stirring) but also by the interaction of the monomers/polymer matrix with the clay lamellar surface (dependent on the extent of its organo-modification).[34−36]

In the present work, the isothermal crystallization kinetics of a series of nanocomposites of PBA synthesized by in situ step growth polycondensation catalyzed by titanium tetrabutoxide in the presence of BDT organically modified with hexadecyltrimethylammonium bromide (CTA) was investigated.[9] The main purpose was to explore the combined effects of molar mass, organoclay content, and CTA/BDT ratio on the isothermal crystallization kinetics of PBA/CTA−BDT nanocomposites. The different extents of nanoclay disaggregation as a result of different organophilicities, defined here by the CTA/BDT ratio, were expected to play a role in the isothermal crystallization rate. On the other hand, to the best of our knowledge the role played by the molecular weight, another variable in the case of nanocomposites prepared by in situ polymerization, in the crystallization kinetics, has never been investigated.[3,4] The isothermal crystallization kinetics of seven different in situ PBA nanocomposites, of the pure PBA matrix synthesized under the same conditions as the nanocomposites, and of the PBA fractions extracted from the nanocomposites, was followed by differential scanning calorimetry (DSC), while the morphology of the nanocomposites was investigated by transmission electron microscopy (TEM), aiming at highlighting a possible specific contribution of the different molecular weights to the crystallization process.

https://doi.org/10.1021/acsapm.1c00684
ACS Appl. Polym. Mater. 2021, 3, 5405−5415

2. EXPERIMENTAL SECTION

2.1. Materials. Adipic acid (AA; Alfa Aesar, 99%), 1,4-butanediol (1,4-BD; Alfa Aesar, 99%), titanium(IV) tetrabutoxide (Aldrich Chemicals, 97%), and hexadecyltrimethylammonium bromide (cetyltrimethylammonium bromide, CTA, Aldrich Chemicals) were used as received without further purification.

Raw ferruginous BDT collected from the Western High Atlas basin of the Agadir region (Morocco)[14] was purified, as previously reported,[9] to obtain homoionic sodium beidellite (Na-BDT) that was sieved to a particle size <2 μm. The specific surface area, porosity, and cation-exchange capacity (CEC) of Na-BDT were assessed to be about 82.2 m^2g^{-1}, 0.136 cm^3g^{-1}, and 58.2 meq·(100 g)$^{-1}$, respectively. The organo-modified BDT clay samples used in this study were prepared by the cation-exchange reaction between Na-BDT and CTA[9] at different CTA/Na-BDT ratios, namely, by using 1, 3, and 5 equivalent ratios of CTA to the CEC of Na-BDT. The three organo-modified BDT clays are labeled hereafter xCTA-BDT, where x can be 1, 3, or 5. All polymerization runs were performed by a two-stage melt polycondensation (esterification followed by polycondensation) between AA and 1,4-BD, with $Ti(OBu)_4$ (titanium tetrabutoxide) as the catalyst. A fraction of each PBA nanocomposite was then treated to separate the polymer from the clay using an ion-exchange and precipitation process. The overall polymerization procedure, as well as the subsequent separation of the nanoclay from the PBA matrix as noted below, has been described in detail in a previous study.[9] One additional sample was prepared as a physical blend by mixing a pure PBA sample, synthesized according to the same procedure adopted for the in situ nanocomposites but without the clay, with 2 wt % of 3CTA-BDT. To this aim, 12 mg of the organo-modified clay was dispersed in 3 mL of $CHCl_3$ with the aid of an ultrasound probe (Hielscher Ultrasonics GmbH mod. UP400 equipped with a 3 mm probe and operated at room temperature for 15 min at 60% power and 1/2 cycle), then 1 mL of such dispersion was added to 3 mL of chloroform solution containing 200 mg of PBA. After 20 min of magnetic stirring, the solvent was quickly removed from the mixture in a rotary evaporator. Hereafter, the nanocomposites will be labeled PBA-y%(Na-BDT) or PBA-y %(xCTA-BDT), where y indicates Na-BDT or xCTA-BDT wt % with respect to the total monomer feed, while the corresponding PBA extracts will be labeled *ex*PBA-y%(Na-BDT) or *ex*PBA-y%(xCTA-BDT), and the blend obtained by solution blending *mix*-PBA. All samples were stored at 4 °C. Altogether, the following samples were investigated: (i) seven pairs of related samples, each pair consisting of a bio-nanocomposite with a given formulation plus the corresponding extracted PBA matrix; (ii) a sample of pure PBA synthesized under the same conditions as the in situ bionanocomposites, but without nanoclay; and (iii) a physical blend prepared by the coprecipitation of the pure PBA with 2 wt % of 2CTA-BDT.

2.2. Methods. Thermogravimetric Analysis (TGA) was carried out with a Mettler Toledo TGA/SDTA 851 instrument at a heating rate of 10 °C·min^{-1} from room temperature to 700 °C, with air as the reactive gas (60 mL·min^{-1}) and nitrogen as the purge gas.

Size exclusion chromatography (SEC) was performed using a Jasco apparatus with a PU-2089 Plus pump and injector, two in series PLgel Mixed-D columns (Polymer Laboratories, Varian, Inc) thermostated at 30 °C in a CO-2063 column oven, a RI-2031 Plus differential refractometry detector, and a UV-2077 Plus UV/vis detector set at 254 nm wavelength. Column calibration was performed with narrow distribution poly(styrene) standards (233, 83, 23.8, and 4.85 kg·mol^{-1}, Polymer Laboratories). The analyses were performed under isocratic conditions at 1 mL/min flow rate of chloroform as the eluent by injecting 20 μL of a 40 mg/mL solution of the polymer previously filtered through a 0.2 μm pore size syringe membrane filter.

DSC measurements were carried out using a TA Instruments DSC 250 Discovery equipped with a refrigerated cooling system 90. Temperature and enthalpy calibrations were performed with indium standards. Samples (5−7 mg) were crimped in aluminum pans. All measurements were performed under a 50 mL/min nitrogen purge. In a typical experiment, the sample was first heated to 90 °C at a rate of 10 °C/min and thermally annealed at this temperature for 30 min to ensure complete melting and erase the thermal history of the sample. Then, the sample was quickly cooled (50 °C/min) to the temperature chosen for the isothermal crystallization process (45, 40, and 37 °C). Finally, a second heating scan up to 90 °C was performed, and the melting temperature was recorded as the peak of the melting endotherm.

The morphology of the nanocomposites was investigated by TEM using an EM 900 transmission electron microscope (Carl Zeiss microscopy GmbH, Jena, Germany) operated at an accelerating voltage of 80 kV. Ultrathin sections (about 50 nm thick) from samples embedded in suitable resin and cooled down to −80 °C were obtained with a Leica EM FCS cryo-ultramicrotome equipped with a diamond knife. Scanning electron microscopy (SEM) analyses were performed using a FEI QUANTA 450 ESEM-FEG at the Centro per la Integrazione della Strumentazione, University of Pisa (CISUP).

3. RESULTS AND DISCUSSION

The pure PBA and the PBA matrices extracted from the nanocomposites were analyzed by SEC to assess the possible effect on the polymer molar mass caused, either directly or indirectly, by the presence of the nanoclay during polycondensation. The latter may provide a support for the initially homogeneous metal catalyst, reactive surfaces interfering or competing with the polymerization reaction, and a physical barrier for the diffusion of the reactive groups involved in polymerization. The molecular weights of the PBA matrices recovered from the nanocomposites were found to be significantly lower than that of the pure PBA obtained under the same reaction conditions adopted for the in situ syntheses with the nanoclays (Table 1), spanning over a broad range without any clear correlation with the organoclay content.

Table 1. Number Average ($\bar{M}_n$) and Weight Average ($\bar{M}_w$) Molecular Weights with the Corresponding Polydispersity *Đ* from SEC Analysis (Relative to a Polystyrene Calibration Curve)

sample	$\bar{M}_n$ (g/mol)	$\bar{M}_w$ (g/mol)	*Đ* ($\bar{M}_w/\bar{M}_n$)
PBA-1%(3CTA-BDT)	4400	8100	1.84
PBA-5%(3CTA-BDT)	7000	13,300	1.90
PBA-2%(Na-BDT)	8500	16,600	1.95
PBA-2%(1CTA-BDT)	9000	18,000	2.00
PBA-2%(5CTA-BDT)	9800	20,000	2.04
PBA-3%(3CTA-BDT)	14,000	28,500	2.04
PBA-2%(3CTA-BDT)	21,000	41,000	1.95
PBA	69,600	120,000	1.72

As already pointed out and discussed in a previous work dealing with some of the nanocomposites studied here,[9] the lower molecular weight of PBA in nanocomposites suggests the occurrence of side reactions either catalyzed by, or otherwise involving, the organo-modified clay. The dependence of the molecular weight on the presence of nanoparticles has been reported for various in situ syntheses.[20−23] In the cited studies, the increase in the nanofiller loading from 0 wt % up to as much as 25 wt % caused a rather regular decrease in the corresponding polymer molar mass, although the reported reduction was generally lower than that observed in our case.

3.1. Morphology of the Nanocomposites and Residual Nanoclay Contaminating the Purified PBA Matrices. In order to focus on the discussion of the results of the morphological analyses, and afterward of the isothermal crystallization experiments, on the specific influence of the

https://doi.org/10.1021/acsapm.1c00684
ACS Appl. Polym. Mater. 2021, 3, 5405−5415

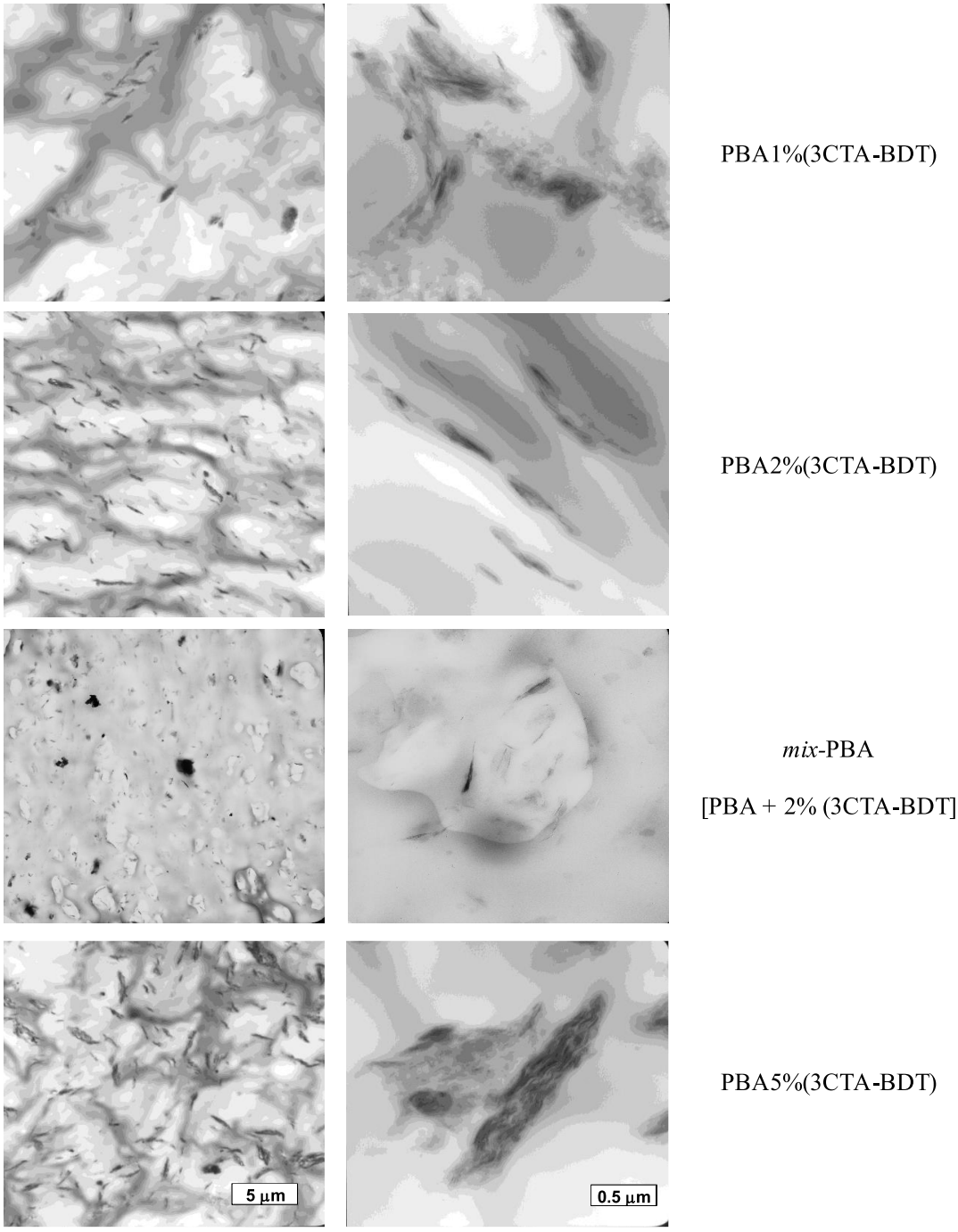

Figure 1. TEM micrographs of group Y nanocomposites. From top: PBA-y%(3CTA-BDT) with y = 1, 2, 2 (*mix*-PBA), 5. Image width: left = 25 μm; right = 2.5 μm (magnification 2000× and 20,000×, respectively).

molecular weight of the PBA matrix, the nanocomposites are conveniently analyzed by considering two distinct groups. In Figure 1 are shown the TEM images taken from the set of nanocomposites containing the same type of organoclay (3CTA-BDT) but in different amounts in the 0−5 wt % range, hereafter collectively labeled as Group Y; the physical blend *mix*-PBA with the same composition as sample PBA-2%(3CTA-BDT) is also included in this group. The TEM micrographs of the nanocomposites containing the same 2 wt % amount of different organoclays (xCTA-BDT with $0 \leq x \leq 5$, that is, including the unmodified Na-BDT; see Figure S1 of the Supporting Information), characterized by different organophilicities and labeled hereafter as Group X, will also be briefly discussed.

It is worth mentioning that the organoclays used in this work were characterized by a substantial, if not exclusive, confinement of CTA in the nanoclay interlayers, resulting in their expansion when an excess CTA with respect to the ion-exchange capacity of the nanoclay was used.[9] An expanded organoclay was expected to promote both catalyst adsorption and clay delamination upon stirring during melt polymerization. Some of the nonelectrostatically bound excess CTA might have desorbed from the clay upon polymerization as a result of shear-induced delamination; however, given the small

https://doi.org/10.1021/acsapm.1c00684
ACS Appl. Polym. Mater. 2021, 3, 5405−5415

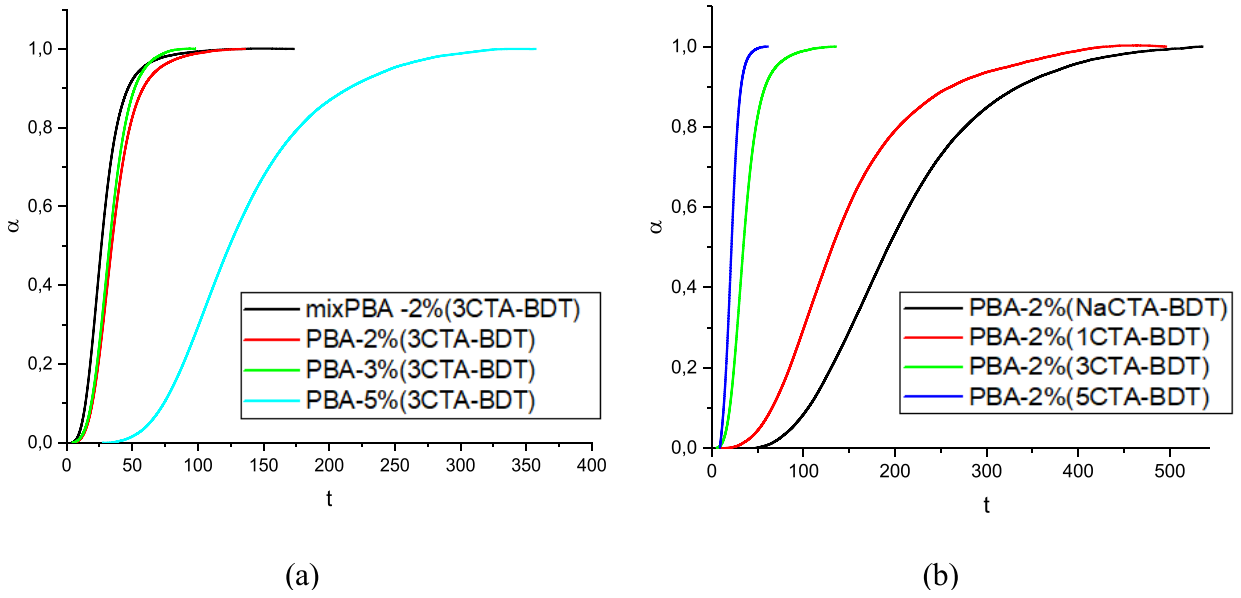

Figure 2. Relative crystallinity $\alpha(t)$ vs time (min), as obtained by DSC measurement isothermal kinetics measurements performed at 45 °C on (a) PBA-y%(3CTA-BDT) nanocomposites (group Y); (b) PBA-2%(xCTA-BDT) nanocomposites (group X).

overall excess CTA (in the 0.4−1.5 wt % range in the final nanocomposites) and its possible partial thermal decomposition into volatile products caused by the high polymerization temperature (220 °C), the presence of traces of free CTA was considered as uninfluential for the final properties of the nanocomposites.

The number of potential nucleating sites in the polymer matrix is expected to increase with the degree of disaggregation of the nanoclay, although single exfoliated lamellae or smaller tactoids have also been reported to be less-effective nucleation sites than the larger aggregates.[37] From the TEM analysis, most of the clay appears to be extensively exfoliated and dispersed in the PBA matrix. In particular, the micrographs of samples from the PBA-y%(3CTA-BDT) series (Group Y, Figure 1) show that the quality of the dispersion of the organo-clay in the PBA matrix is dependent not only on the extent of organophilic modification (Figure S1 of the Supporting Information) but also on the content of organoclay in the nanocomposite. At low nanoclay content, the presence of tactoids with different sizes and nonuniform distribution within the matrix can be clearly noticed. At intermediate 2 wt % of clay, the volume distribution of tactoids becomes more uniform and their dispersion improves. The reference *mix*-PBA nanocomposite with the same composition as PBA-2%(3CTA-BDT), but prepared by physical blending of the polymer matrix with the nanoclay through solvent-nonsolvent coprecipitation, does not show significant differences in the quality of the nanoclay dispersion and exfoliation. Further increase in the clay content does not lead to further improvements in the clay dispersion; in fact, the sample with 5 wt % of 3CTA-BDT shows the presence of aggregates larger than 1 μm and of submicrometric tactoids with 20 or more layers. Similar morphologies had already been reported for the analogous nanocomposites poly(ε-caprolactone)-y%(3CTA-BDT).[15]

In order to assess the exhaustiveness of the extraction procedure of the CTA−BDT nanofiller from the nanocomposites, the *ex*PBA samples obtained after precipitation and separation of the nanofiller were analyzed by thermogravimetry. While the residues after thermal decomposition at 700 °C of the organic fraction matched well the nominal nanoclay content (see Figure S2 and Table S1 of the Supporting Information), the residues in the purified PBA always fall below 1 wt %, that is, within the uncertainty of about ±1% affecting our TGA measurements. The good efficacy of the adopted purification procedure was further checked by performing filtration of diluted chloroform solutions of the purified PBA samples through a 0.2 μm pore size nylon membrane and by checking the membrane surface for the possible presence of nanoclay residues not completely removed from the polymer matrix during the purification process. SEM analyses and EDS microanalyses of the surface of the membrane allowed detection of only a few scattered particles, some of which were actually the result of environmental contamination (e.g., airborne particulate), along with a few clay particles (see Figure S3 and Figure S4 of the Supporting Information).

3.2. Isothermal Crystallization Kinetics Based on the Avrami Model. The isothermal crystallization study was based on DSC measurements. The results of the thermal characterization of the nanocomposites and of the *ex*PBA matrices can be found in the Supporting Information (representative DSC thermograms are shown in Figure S5; thermal parameters are shown in Table S2; a plot of T_m against the PBA molecular weights is shown in Figure S6, where the presence of a threshold value at about $\bar{M}_w$ = 20,000 g/mol marks a possible similar threshold in other nanocomposite properties).

Under isothermal conditions, the polymer crystallization kinetics is described with a generally good accuracy, at least for the early stage of the process, by the Avrami model according to eq 1:[38−40]

$$\alpha(t) = 1 - \exp[-K(t - t_0)^n] \quad (1)$$

where $\alpha(t)$ is the relative crystallinity at time t; t_0 is a parameter required to match the effective beginning of the isothermal crystallization process; K is a crystallization rate constant, which depends on the crystallization temperature and on the geometry of the sample; n is the so-called Avrami

https://doi.org/10.1021/acsapm.1c00684
ACS Appl. Polym. Mater. 2021, 3, 5405−5415

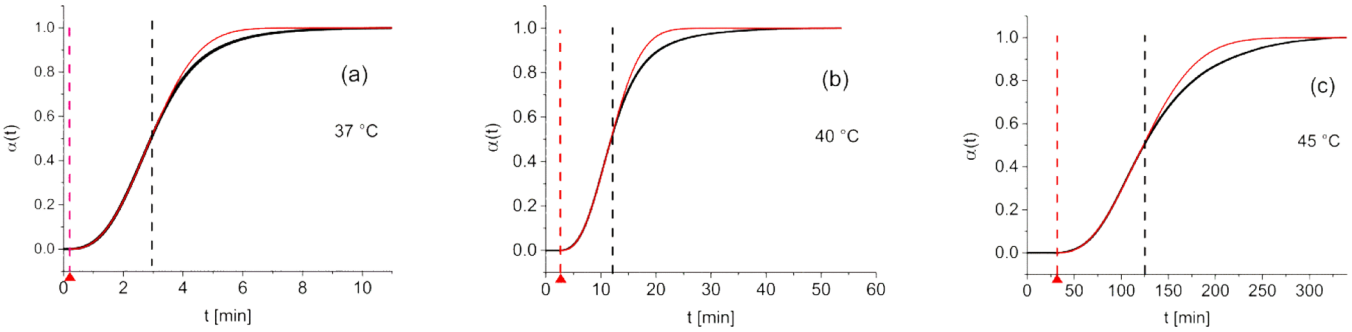

Figure 3. Avrami best fit (red line) of the experimental $\alpha(t)$ values (black points) for PBA-5%(3CTA-BDT) at 37 °C (a), 40 °C (b), and 45 °C (c). In each graph, the starting point of the crystallization process, determined by the best-fit parameter t_0 of the Avrami model, is indicated by the red arrow; the fitting procedure was performed on the experimental values in the range $0 < \alpha(t) < 0.5$, included between the vertical dashed lines. Note the different time ranges on the horizontal axis because of the different crystallization rates.

Table 2. Avrami Parameters for PBA and for *ex*PBA Matrices Extracted from the Nanocomposites, Listed by Increasing $\bar{M}_w$

sample	t_0 (min)			n			K (10^{-4} min)$^{-n}$		
nanocomposites	45 °C	40 °C	37 °C	45 °C	40 °C	37 °C	45 °C	40 °C	37 °C
PBA-1%(3CTA-BDT)	[a]	15.2	1.37	-	1.99	2.37	-	1.68	15.0
PBA-5%(3CTA-BDT)	34.1	2.82	0.196	2.31	2.39	2.51	0.216	36.6	558
PBA-2%(Na-BDT)	44.9	2.08	−0.269	2.09	2.16	2.73	0.204	70.6	548
PBA-2%(1CTA-BDT)	18.2	1.21	0.00	2.16	2.80	2.65	0.262	20.1	640
PBA-2%(5CTA-BDT)	5.79	−0.239	−0.314	2.84	3.01	3.27	2.27	26.6	2252
PBA-3%(3CTA-BDT)	3.39	0.09	−0.496	2.96	2.70	2.83	0.321	252	2410
PBA-2%(3CTA-BDT)	5.18	0.472	−0.191	2.67	2.52	2.84	0.856	166	1195
mix-PBA	4.30	0.319	−0.16	2.39	1.80	2.40	4.28	1057	2592
exPBA matrices									
PBA	4.30	1.15	−0.139	2.39	2.41	2.23	3.53	58.6	632
PBA-1%(3CTA-BDT)	N.D.[a]	4.15	0.00		2.06	2.58		9.48	37.4
PBA-5%(3CTA-BDT)	25.0	2.80	3.10	2.08	2.43	2.42	0.213	11.7	393
PBA-2%(Na-BDT)	22.8	5.11	0.195	2.58	2.28	2.37	0.0686	15.0	179
PBA-2%(1CTA-BDT)	15.2	0.662	−0.250	2.73	2.47	2.95	0.372	54.5	947
PBA-2%(5CTA-BDT)	15.4	1.21	−0.218	2.76	2.55	2.51	0.0761	13.9	166
PBA-3%(3CTA-BDT)	5.77	0.00	−0.303	2.55	2.40	3.13	2.35	312	1243
PBA-2%(3CTA-BDT)	4.98	0.172	−0.492	2.87	2.66	3.22	0.284	66.3	329

[a]N.D.= Not determined as it was larger than 8 h

exponent, related to the time dependence of the nucleation rate and to the dimensionality of the crystal growth.[41,42] Here, time is measured from the moment when the temperature set for the isothermal crystallization process has been reached; at the end of the process, corresponding to the stabilization of the normalized heat flow in the DSC experiment, the value of α will be 1. The longer the delay time (the time between the start of the measurement, following the stabilization of the temperature in the DSC cell, and the t_0 value corresponding to the actual beginning of the crystallization process) the slower was generally observed to be the kinetics. On the other hand, in case of very fast kinetics, the crystallization process might begin before the stabilization of the temperature, with a corresponding negative value of t_0. The different t_0 values in the DSC curves can be clearly observed in the thermograms of Figure S5 in the Supporting Information.

From the DSC thermograms of the isothermal kinetics experiments, the relative crystallinity $\alpha(t)$ can be calculated according to eq 2:

$$\alpha(t) = \frac{\Delta H_{(t)}}{\Delta H_{(\mathrm{tot})}} \qquad (2)$$

where $\Delta H_{(\mathrm{tot})}$ is the total enthalpy loss resulting from the isothermal crystallization process, and $\Delta H_{(t)}$is the enthalpy loss from the beginning of the process to time t.

Among the group Y nanocomposites, the crystallization rate for PBA-5%(3CTA-BDT) was by far the lowest, as shown by the time evolution of α(t) in Figure 2a. In Figure 2b, the same graph for group X nanocomposites shows slower processes for the less organophilic nanocomposites (CTA/BDT equivalent ratio of 0 and 1). In both groups, only the slowest processes present an initial period of latency.

The following quantitative analysis is based on the fitting of the α(t) data sets by eq 1. It is well known that the Avrami model describes in a generally accurate way the first part of the crystallization process (typically up to α values of 30 to 60%[40]), while in the final stage, the so-called secondary crystallization mechanism prevails.[43] In all cases analyzed in this work, the overlap of the Avrami fit with the experimental points throughout the first half of the isothermal crystallization process is excellent (nonlinear fitting performed with Origin Pro 2015 Data Analysis and Graphing Software, based on the Levenberg−Marquardt algorithm[44]). This is clearly shown in three plots reported in Figure 3, representative of progressively slower crystallization processes at increasing crystallization

https://doi.org/10.1021/acsapm.1c00684
ACS Appl. Polym. Mater. 2021, 3, 5405−5415

Table 3. Isothermal Crystallization Rate Parameters (Derived from the Avrami Parameters) for the Nanocomposites and the *ex*PBA Matrices

		$t_{1/2}$ (min)						v (10^{-2} min^{-1})					
		PBA[a]			nanocomposites			PBA[a]			nanocomposites		
sample composition	$\bar{M}_w$ (g/mol)	45 °C	40 °C	37 °C	45 °C	40 °C	37 °C	45 °C	40 °C	37 °C	45 °C	40 °C	37 °C
PBA-1%(3CTA-BDT)	8100		24.5	7.57		65.0	13.3	-	4.09	13.2		1.54	7.52
PBA-5%(3CTA-BDT)	13,300	148	13.9	3.28	89.1	9.05	2.72	0.68	7.19	30.5	1.12	11.1	36.7
PBA-2%(Na-BDT)	16,600	86.6	14.7	3.45	147	8.36	2.39	1.15	6.78	29.0	0.68	12.0	41.8
PBA-2%(1CTA-BDT)	18,000	57.7	7.12	1.93	112	8.08	2.46	1.73	14.0	51.8	0.90	12.4	40.7
PBA-2%(5CTA-BDT)	20,000	62.8	11.4	4.42	16.9	6.39	1.41	1.59	8.77	22.6	5.93	15.7	70.9
PBA-3%(3CTA-BDT)	28,500	23.0	3.63	2.59	29.0	3.41	1.73	4.35	27.5	38.6	3.45	29.0	57.8
PBA-2%(3CTA-BDT)	41,000	34.0	5.73	2.58	29.1	4.36	1.86	2.94	17.5	38.8	3.44	23.0	53.8
PBA	120,000	25.4	7.25	2.93				3.94	13.8	34.1			
mix-PBA	120,000				22.1	2,84	1.51				4.52	35,2	66.4

[a]Extracted PBA from nanocomposites and pure PBA used in the *mix*-PBA physical blend.

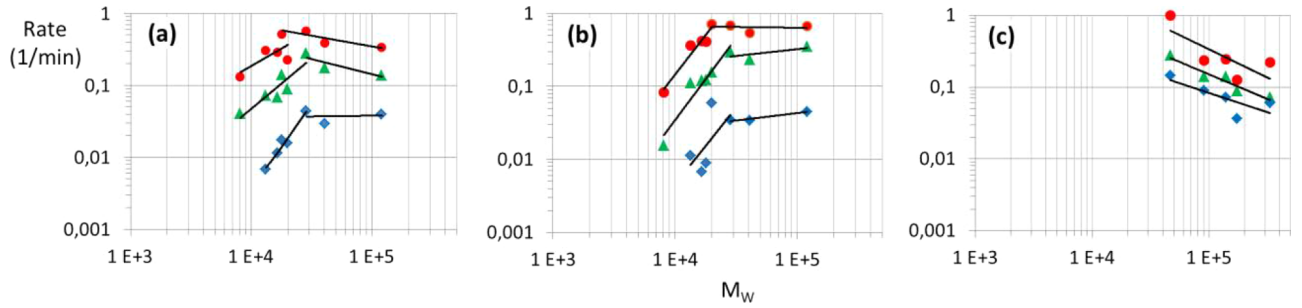

Figure 4. Isothermal crystallization rate vs molecular weight: (a) PBA (extracted polymers from the nanocomposites, and pure PBA used for the physical blend): blue diamonds, T = 45 °C; green triangles, T = 40 °C; red circles, T = 37° C; (b) nanocomposites: symbols for the isothermal crystallization temperatures as in (a); (c) linear or branched PBA:[5] blue diamonds, T = 42 °C; green triangles, T = 40 °C; red circles, T = 38 °C.

temperature. In each graph, for $\alpha(t) > 0.5$, the Avrami equation which best fits the data in the $0 < \alpha(t) < 0.5$ range diverges from the experimental trend. For each $\alpha(t)$ data set ($0 < \alpha(t) < 0.5$), typically including a few thousands of experimental points, three best-fit parameters, t_0, K, and n, were determined, as listed in Table 2 (the reported values are the averages calculated from repeated experiments, which always gave well reproducible results).

As expected, t_0 assumes quite high values for the samples crystallized at 45 °C, characterized by very slow kinetics. The fitting procedure confirmed that the crystallization process follows the Avrami model since its very beginning, when the heat release is first detected. Slightly negative values of t_0 have been obtained for several of the faster kinetics because of the time lapse for the instrumental equilibration before the heat flow data could start to be collected. For all samples, values of $2 < n < 3$ or slightly above this range were determined, suggesting simultaneous homogeneous and heterogeneous nucleation during crystallization and primarily two-dimensional crystal growth. The highest values were obtained at the lowest tested temperature (37 °C) and from the fastest crystallizing samples, for which three-dimensional crystal growth may be the dominant process.[41,42]

The values of the rate constant K are spread over several orders of magnitude for both the nanocomposites and the extracted PBA, from about 10^{-5} to about 10^{-1} min^{-n}, lower values corresponding to slower kinetics (typically those at 45 °C). However, because n differs for various samples, it is not appropriate to discuss the crystallization rates by simply comparing the values of K. A more appropriate and commonly used measure of the crystallization rate is the reciprocal of the crystallization half-time, $v = (1/t_{1/2})$, as $t_{1/2}$ can be calculated from K and n by eq 3:

$$t_{1/2} = \left(\frac{\ln 2}{K}\right)^{1/n} \tag{3}$$

The calculated $t_{1/2}$ and v values are listed in Table 3.

In the following, the trends of the isothermal crystallization rates will be analyzed in detail, aiming at untangling, and possibly rationalizing, in particular, the influence of the PBA molecular weight, along with the contributions of the content (y%) of the CTA−BDT nanoclay in the nanocomposite and that of the CTA (x) equivalent ratio in the organoclay.

3.3. Effect of the Molecular Weight on the Isothermal Crystallization Rate. As a general rule, the isothermal crystallization rate of polymers is hardly detectable over any reasonable measurement time at temperatures just below T_m. As the temperature is lowered, the rate progressively increases, goes through a maximum, and then decreases again, going to zero below the glass transition temperature.[45] The isothermal crystallization rates were recorded for PBA and for the PBA extracts from the nanocomposites at three different temperatures (see the plotted data in Figure S7 in the Supporting Information) in a temperature range close enough to the melting temperature to result in increasing crystallization rates with decreasing temperature.

The trends of the isothermal crystallization rates as a function of $\bar{M}_w$, as reported for various polymers,[46,47] present substantially common features, with the crystallization rate rapidly increasing with $\bar{M}_w$ until a threshold value is reached at molecular weights most often observed in the range between

https://doi.org/10.1021/acsapm.1c00684
ACS Appl. Polym. Mater. 2021, 3, 5405−5415

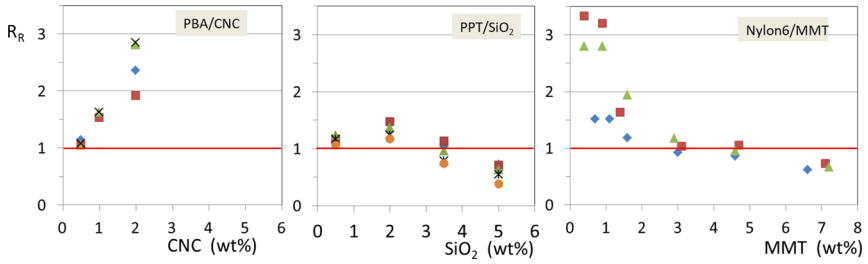

Figure 5. Ratios R_R between the isothermal crystallization rate of the pure polymer and that of the corresponding nanocomposites prepared by physical blending, at various nanofiller loadings. Left: PBA with acicular nanocellulose (different symbols refer to temperatures in the 38−44 °C range; adapted from ref 3.); center: poly(propylene terephthalate) with spheroidal nanosilica (different symbols refer to temperatures in the 184−200 °C range; adapted from ref 30.); and right: nylon 6 of various molecular weights (blue diamonds, 16.3 kg/mole; green triangles, 22.0 kg/mole; red squares, 29.4 kg/mole) with organo-modified montmorillonite (adapted from ref 31.).

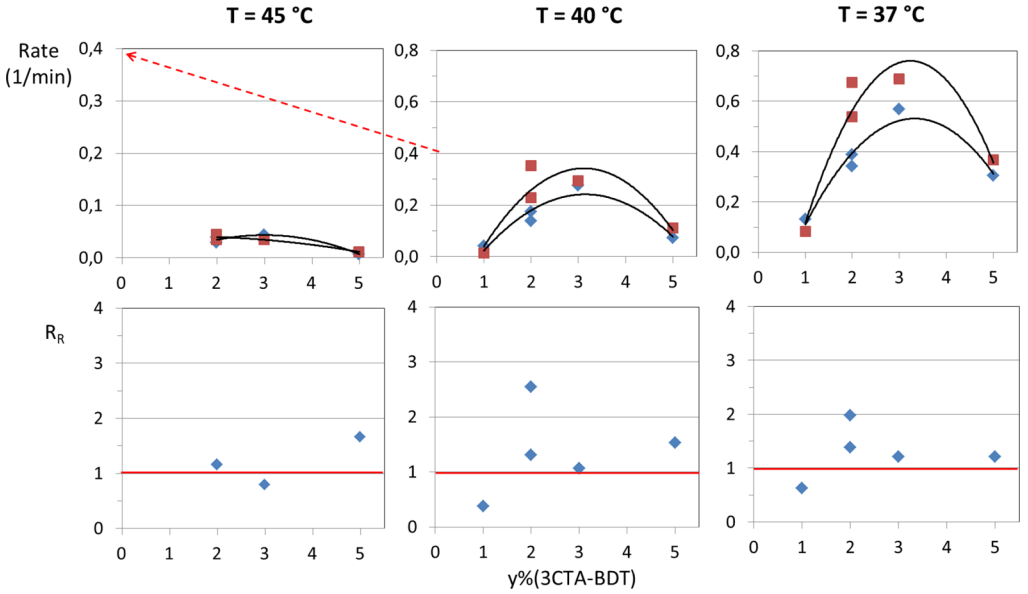

Figure 6. Top graphs: isothermal crystallization rates of group Y nanocomposites with 3CTA-BDT(red squares), and of the corresponding *ex*PBA matrices (blue diamonds), plotted against the organoclay content (curves shown as a visual aid). Bottom graphs: ratios R_R between the isothermal crystallization rates for each nanocomposite/*ex*PBA pair. From left to right: data collected at decreasing isothermal crystallization temperature, namely, 45 °C (note the expansion of the vertical scale, as highlighted by the dashed arrow), 40 °C, and 37 °C.

10,000 and 20,000 g/mol (see Figure S8 in the Supporting Information for linear polyethylene). Indeed, a similar behavior can also be observed in the log−log plots of Figure 4 relative to the experiments performed on the PBA matrices of this investigation and on the corresponding nanocomposites, as well as on other PBA matrices.[5]

The graphs in Figure 4a,b strictly resemble those included in the red circle of Figure S8 in the Supporting Information,[46] with an apparent discontinuity around $\bar{M}_w$ = 20,000 g/mole, marking the difference between a lower molar mass range, in which the crystallization rate increases with increasing $\bar{M}_w$, and a higher molecular weight range, in which the crystallization rate is stabilized or decreases slightly with increasing $\bar{M}_w$. In fair agreement with these findings, a decrease in the isothermal crystallization rate with increasing $\bar{M}_w$ had been reported for linear and branched PBA with $\bar{M}_w$ >40,000 g/mole (see Figure 4c).[5] By comparing the two graphs in Figure 4a,b , it is also apparent that the presence of the nanoclay in the nanocomposites affects the crystallization rate of the PBA matrix, slowing down the rate for the PBA matrices with lower $\bar{M}_w$ (possibly as a result of hindered diffusion of highly mobile macromolecular chains), but increasing the rate for the PBA matrices with higher $\bar{M}_w$ (possibly due to assisted nucleation for macromolecular chains that are less mobile as they are likely above the entanglement threshold). Anyway, it is clear that the isothermal crystallization rate of nanocomposites is influenced by the sample's molecular weight, in combination with other factors such as the crystallization temperature, the nature (size, shape, and surface chemistry), the concentration, and the quality of the dispersion of the nanofiller.

3.4. Singling out the Influence of the Molecular Weight and That of the Nanoclay Loading on the Crystallization Kinetics of the PBA/Nanoclays. In the literature, various sets of data relative to nanocomposites based on physical blends with the same polymer matrix (or with matrices having very similar molecular weights) can be found. In such cases, a rather straightforward relationship between the isothermal crystallization rate and the nanofiller content is generally observed.[3,30,31] Typically, the addition of small quantities of nanofiller increases the crystallization rate with respect to that of the pure polymer matrix as a result of heterogeneous nucleation. However, above a given threshold, a further increase of the amount of nanofiller results in the reduction of the crystallization rate even below that of the pure

https://doi.org/10.1021/acsapm.1c00684
ACS Appl. Polym. Mater. 2021, 3, 5405−5415

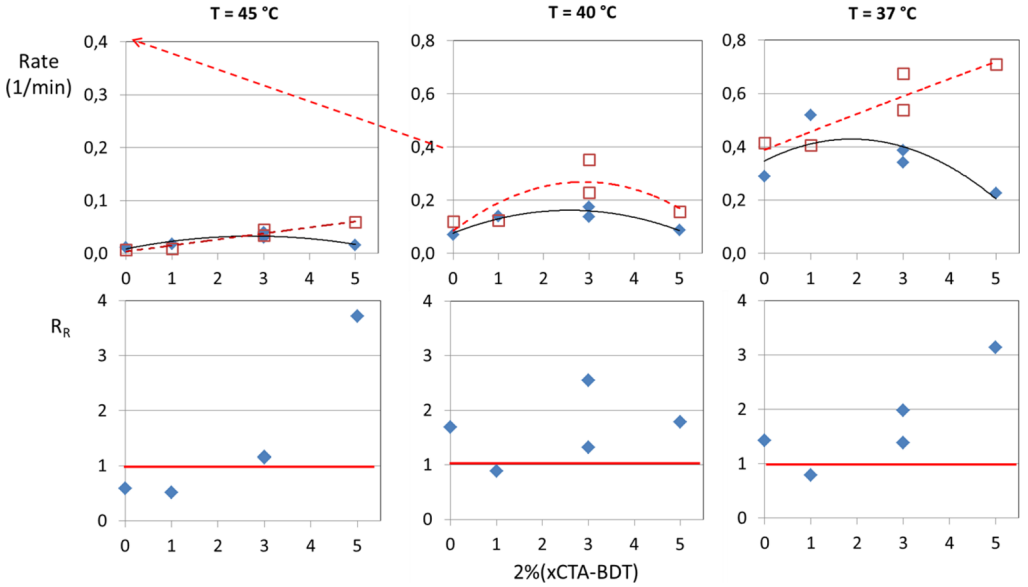

Figure 7. Top graphs: isothermal crystallization rates of group Y nanocomposites containing 2 wt % of different nanoclays (red hollow squares) and of the *ex*PBA matrices (blue diamonds), plotted against the organoclay content (curves shown as a visual aid). Bottom graphs: ratios R_R between the isothermal crystallization rates for each nanocomposite/*ex*PBA pair. From left to right: data collected at decreasing temperatures, namely, 45 °C (note the expansion of the vertical scale, as highlighted by the dashed arrow), 40 °C, and 37 °C.

polymer. This is clearly highlighted in the central graph of Figure 5, a similar behavior having also been reported for poly(L-lactide) and poly(butylene succinate-*co*-adipate) bio-nanocomposites with organo-modified layered double hydroxide.[28,29] Such a threshold had probably not been reached in the system described in the left graph of Figure 5, while it might have been below the lowest investigated nanofiller loading range in the right graph (a similar behavior has been described for PBA with organo-modified layered double hydroxide[4]). Note that nanocellulose, silica, and claylike layered nanoparticles have quite different aspect ratios and surface chemical compositions.

As anticipated in Section 3.1, the results of our isothermal crystallization experiments are conveniently analyzed by separately discussing the samples of group Y (those with the same 3CTA-BDT organoclay but in different amounts) and those of group X (nanocomposites with 2 wt % of different nanoclays, namely, the pristine Na-BDT and the three xCTA-BDT), along with the corresponding extracted PBA.

The isothermal crystallization rates of group Y nanocomposites are compared with those of their corresponding PBA matrices in Figure 6. Differently from the above cited cases from the literature, the rate ratio R_R (ratios between the isothermal crystallization rates for each nanocomposite/PBA matrix pair) does not show any correlation with the organoclay content, the only common feature being a consistently slower crystallization rate in the nanocomposites ($R_R < 1$) at the lowest 1 wt % content of nanoclay. This is likely a result of the different contributions from the density of nucleation sites increasing with increasing nanoclay concentration, and the molecular weights of the parent PBA matrices being uncorrelated with the nanoclay concentration.

In Figure 7, the isothermal crystallization rates of group X nanocomposites are compared with those of their corresponding PBA matrices. Again, the presence of xCTA-BDT or Na-BDT (corresponding to $x = 0$) in the PBA matrix causes, in most cases, an increase in the crystallization rate. However, in this series, an apparently more regular increase in the crystallization rate is observed upon increasing organophilicity of the nanoclay, the latter being probably associated with increasing extent of the delamination/exfoliation of the lamellar stacks of nanoclay, which in turn may result in enhanced nucleation and thus faster crystallization. Incidentally, in these samples, the molecular weights of the PBA matrices increase along with the content of the CTA modifier in the organoclay, with the exception of sample PBA-2%(5CTA-BDT) in which the PBA matrix has a lower molecular weight than PBA-2%(3CTA-BDT). However, the value of $\bar{M}_w$ = 20,000 g/mole for *ex*PBA-2%(5CTA-BDT) matches the previously discussed threshold, above which the influence of the molecular weight becomes negligible or even reversed, providing a further evidence of a nontrivial effect of the molecular weight on some relevant physical properties (further arguments supporting such evidence can be found in the comments in Figure S9 of the Supporting Information).

4. CONCLUSIONS

The molecular weights of PBA synthesized by in situ step growth catalytic polycondensation were found to be affected by the presence of the nanoclay, causing a generalized reduction of it to a different extent, although such reduction was not correlated with the extent of nanoclay modification. The latter affects the extent of delamination/exfoliation of the nanoclay, as highlighted by the different morphologies of the nanoclay dispersion in the final bionanocomposites. However, the most significant result of the present investigation concerns the pinpointing of a specific contribution of the molecular weight in determining the crystallization rate. The latter, along with the crystallinity and crystal morphology, may affect application-relevant properties of the bio-nanocomposite such as mechanical strength, barrier properties, and biodegradability, to mention a few. In fact, while the type and concentration of the nanofiller are generally investigated as the factors affecting the crystallization rate in nanocomposites (most frequently produced by melt mixing or solvent coprecipitation of the

https://doi.org/10.1021/acsapm.1c00684
ACS Appl. Polym. Mater. 2021, 3, 5405−5415

same polymer matrix with different amounts/types of nanofillers), the results presented here indicate that also the molecular weight plays a not-negligible role, similar to what had been already observed for several pure polymers, but only incidentally for nanocomposites. As a consequence, while in situ polymerization may result in possibly better properties of the nanocomposite associated with improved nanofiller dispersion/delamination, it may also lead to less easily predictable ones as these may also be affected by the molecular weight of the newly synthesized polymer matrix.

The isothermal crystallization kinetics of the investigated PBA/BDT-CTA bionanocomposites followed quite well the Avrami model, with the crystallization rates showing nonlinear variations with the molecular weight. In particular, a trend similar to that of pure polymeric matrices was observed, that is, with a maximum rate reached above the entanglement threshold, irrespective of the temperature at which the isothermal crystallization experiment is carried out.

■ ASSOCIATED CONTENT

Supporting Information

The Supporting Information is available free of charge at https://pubs.acs.org/doi/10.1021/acsapm.1c00684.

(i) TEM analysis of Group X nanocomposites; (ii) evaluation of the possible presence of residual nanoclay in the purified PBA samples by minutes of thermogravimetric and SEM analyses; (iii)thermal analysis; and (iv) effect of the molecular weight on the isothermal crystallization rate. (PDF)

■ AUTHOR INFORMATION

Corresponding Author

Valter Castelvetro − *Department of Chemistry and Industrial Chemistry, University of Pisa, 56124 Pisa, Italy;* orcid.org/0000-0002-3302-7037; Email: valter.castelvetro@unipi.it

Authors

Donata I. M. Catalano − *Department of Chemistry and Industrial Chemistry, University of Pisa, 56124 Pisa, Italy*

Lucia Conzatti − *Institute of Chemical Science & Technology "Giulio Natta", National Research Council (CNR-SCITEC), 16149 Genoa, Italy;* orcid.org/0000-0003-1899-8262

Mohamed Ilsouk − *IMED-Lab, Faculty of Sciences and Technologies, Cadi-Ayyad University, 40000 Marrakech, Morocco;* orcid.org/0000-0003-0800-3233

Mohamed Lahcini − *IMED-Lab, Faculty of Sciences and Technologies, Cadi-Ayyad University, 40000 Marrakech, Morocco;* orcid.org/0000-0003-1049-7906

Antonella Manariti − *Department of Chemistry and Industrial Chemistry, University of Pisa, 56124 Pisa, Italy*

Elena Maurina − *Department of Chemistry and Industrial Chemistry, University of Pisa, 56124 Pisa, Italy*

Mustapha Raihane − *IMED-Lab, Faculty of Sciences and Technologies, Cadi-Ayyad University, 40000 Marrakech, Morocco*

Benaissa Rhouta − *IMED-Lab, Faculty of Sciences and Technologies, Cadi-Ayyad University, 40000 Marrakech, Morocco*

Complete contact information is available at: https://pubs.acs.org/10.1021/acsapm.1c00684

Author Contributions

The manuscript was written through contributions of all authors. All authors have given approval to the final version of the manuscript.

Notes

The authors declare no competing financial interest.

■ ACKNOWLEDGMENTS

Financial support for cooperative research came from the MESRSFC and CNRST of Morocco (PPR program), the University of Pisa (International Academic Cooperation Support Action Program-Cooperation with the University Cadi Ayyad of Marrakech), the CNRST (Morocco)-CNR (Italy) program, and the Hassan II Academy of Science and Technology of Morocco/CSIC-Spain (Project AH11STC-nano and 2010MA003). Scanning electron microscopy analyses were performed using a FEI QUANTA 450 ESEM-FEG at the Centro per la Integrazione della Strumentazione-University of Pisa (CISUP).

■ REFERENCES

(1) Abe, H.; Doi, Y.; Aoki, H.; Akehata, T. Solid-State Structures and Enzymatic Degradabilities for Melt-Crystallized Films of Copolymers of (R)-3-Hydroxybutyric Acid with Different Hydroxyalkanoic Acids. *Macromolecules* **1998**, *31*, 1791.

(2) Pan, P.; Inoue, Y. Polymorphism and isomorphism in biodegradable polyesters. *Prog. Polym. Sci.* **2009**, *34*, 605−640.

(3) Ye, H.-M.; Wang, C.-S.; Zhang, Z.-Z.; Yao, S.-F. Effect of cellulose nanocrystals on the crystallization behavior and enzymatic degradation of poly(butylene adipate). *Carbohydr. Polym.* **2018**, *189*, 99−106.

(4) Chen, Y.-A.; Hang, Y.-T.; Wu, T.-M. Polymorphism and spherulite morphology of poly(1,4-butylene adipate)/organically-modified layered double hydroxide nanocomposites. *J. Appl. Polym. Sci.* **2015**, *132*, 42526.

(5) Chae, H. G.; Kim, B. C.; Im, S. S.; Han, Y. K. Effect of molecular weight and branch structure on the crystallization and rheological properties of poly(butylene adipate). *Polym. Eng. Sci.* **2001**, *41*, 1133−1139.

(6) Saeidlou, S.; Huneault, M. A.; Li, H.; Park, C. B. Poly(lactic acid) crystallization. *Prog. Polym. Sci.* **2012**, *37*, 1657−1677.

(7) Papageorgiou, G.; Achilias, G.; Bikiaris, D. Crystallization Kinetics of Biodegradable Poly(butylene succinate) under Isothermal and Non-Isothermal Conditions. *Macromol. Chem. Phys.* **2007**, *208*, 1250−1264.

(8) Ren, M. Q.; Song, J. B.; Song, C. L.; Zhang, H. L.; Sun, X. H.; Chen, Q. Y.; Zhang, H. F.; Mo, Z. S. Crystallization kinetics and morphology of poly(butylene succinate-co-adipate). *J. Polym. Sci. B* **2005**, *43*, 3231−3241.

(9) Ilsouk, M.; Raihane, M.; Castelvetro, V.; Lahcini, M.; Bronco, S.; Rhouta, B.; Bianchi, S.; Conzatti, L. Highly thermostable and crystalline poly(butylene adipate) bionanocomposites prepared by in situ polycondensation with organically modified Moroccan beidellite clay. *Polym. Int.* **2017**, *66*, 939−949.

(10) Raffa, P.; Coltelli, M.-B.; Castelvetro, V. Expanding the application field of post-consumer poly(ethylene terephthalate) through structural modification by reactive blending. *J. Appl. Polym. Sci.* **2014**, *131*, 40881.

(11) Reddy, M. M.; Vivekanandhan, S.; Misra, M.; Bhatia, K. S.; Mohanty, A. K. Biobased plastics and bionanocomposites: Current status and future opportunities. *Prog. Polym. Sci.* **2013**, *38*, 1653−1689.

(12) Mittal, V. Polymer Layered Silicate Nanocomposites: A Review. *Dent. Mater.* **2009**, *2*, 992−1057.

(13) Ray, S. S.; Okamoto, M. Polymer/layered silicate nanocomposites: a review from preparation to processing. *Prog. Polym. Sci.* **2003**, *28*, 1539−1641.

(14) Bouna, L.; Rhouta, B.; Daoudi, L.; Maury, L.; Amjoud, M.; Senocq, F.; Lafont, M. C.; Jada, A.; Aghzzaf, A. A. Mineralogical and Physico-Chemical Characterizations of Ferruginous Beidellite-Rich Clay from Agadir Basin (Morocco). *Clays Clay Miner.* **2012**, *60*, 278−290.
(15) Ilsouk, M.; Raihane, M.; Lahcini, M.; Meri, R. M.; Zicans, J.; Cimdina, L. B.; Kharas, G. B. Bionanocomposites poly(ϵ-caprolactone)/organomodified Moroccan beidellite clay prepared by in situ ring opening polymerization: Characterizations and properties. *J. Macromol. Sci., Part A: Pure Appl. Chem.* **2017**, *54*, 201−210.
(16) Ilsouk, M.; Raihane, M.; Rhouta, B.; Meri, R. M.; Zicans, J.; Vecstaudža, J.; Lahcini, M. The relationship of structure, thermal and water vapor permeability barrier properties of poly(butylene succinate)/organomodified beidellite clay bionanocomposites prepared by *in- situ* polycondensation. *RSC Adv.* **2020**, *10*, 37314−37326.
(17) Ezzeddine, I.; Ghorbel, N.; Ilsouk, M.; Arous, M.; Lahcini, M.; Bouharras, F. Z.; Raihane, M.; Kallel, A. Dielectric and thermal characteristics of Beidellite nanoclay-reinforced poly(butylene succinate). *Mater. Chem. Phys.* **2021**, *258*, No. 123855.
(18) Castelvetro, V.; De Vita, C. Nanostructured Hybrid Materials from Aqueous Polymer Dispersions. *Adv. Colloid Interface Sci.* **2004**, *108-109*, 167−185.
(19) Kotal, M.; Bhowmick, A. K. Polymer nanocomposites from modified clays: Recent advances and challenges. *Prog. Polym. Sci.* **2015**, *51*, 127−187.
(20) Pospiech, D.; Korwitz, A.; Komber, H.; Voigt, D.; Jehnichen, D.; Müller, J.; Janke, A.; Hoffmann, T.; Kretzschmar, B. In situ Synthesis of Poly(ethylene terephthalate)/layered Silicate Nanocomposites by Polycondensation. *High Perf. Polym.* **2007**, *19*, 565−580.
(21) Kostoglou, M.; Bikiaris, D. Kinetic Analysis of Nanocomposites Prepared in situ Consisting of an Aliphatic Biodegradable Polyester and Fumed Silica Nanoparticles. *Macromol. React. Eng.* **2011**, *5*, 178−189.
(22) Wei, Z.; Wang, G.; Wang, P.; Liu, L.; Qi, M. Crystallization behavior of poly(ϵ-caprolactone)/TiO_2nanocomposites obtained by in situ polymerization. *Polym. Eng. Sci.* **2012**, *52*, 1047−1057.
(23) Katiyar, V.; Gerds, N.; Koch, C. B.; Risbo, J.; Hansen, H. C. B.; Plackett, D. Poly l-lactide-layered double hydroxide nanocomposites via in situ polymerization of l-lactide. *Polym. Degrad. Stab.* **2010**, *95*, 2563−2573.
(24) Shehzad, F.; Daud, M.; Al-Harthi, M. A. Synthesis, characterization and crystallization kinetics of nanocomposites prepared by in situ polymerization of ethylene and graphene. *J. Therm. Anal. Calorim.* **2016**, *123*, 1501−1511.
(25) Terzopoulou, Z.; Baciu, D.; Gounari, E.; Steriotis, T.; Charalambopoulou, G.; Bikiaris, D. Biocompatible Nanobioglass Reinforced Poly(ϵ-Caprolactone) Composites Synthesized via In Situ Ring Opening Polymerization. *Polymer* **2018**, *10*, 381.
(26) Mandelkern, L. *Crystallization kinetics of homopolymers: Bulk crystallization. In: Crystallization of Polymers*; Cambridge University Press: Cambridge, 2004. Vol. 2, p. 58, and references therein.
(27) Yang, J.; Pan, P.; Dong, T.; Inoue, Y. Crystallization kinetics and crystalline structure of biodegradable Poly(ethylene adipate). *Polymer* **2010**, *51*, 807−815.
(28) Pan, P.; Zhu, B.; Dong, T.; Inoue, Y. Poly(L-lactide)/layered double hydroxides nanocomposites: Preparation and crystallization behavior. *J. Polym. Sci. B* **2008**, *46*, 2222−2233.
(29) Chen, Y.-A.; Tsai, G.-S.; Chen, E.-C.; Wu, T.-M. Crystallization behaviors and microstructures of poly(butylene succinate-co-adipate)/modified layered double hydroxide nanocomposites. *J. Mater. Sci.* **2016**, *51*, 4021−4030.
(30) Achilias, D. S.; Bikiaris, D. N.; Papastergiadis, E.; Giliopoulos, D.; Papageorgiou, G. Z. Characterization and Crystallization Kinetics of in situ Prepared Poly(propyleneterephthalate)/SiO_2 Nanocomposites. *Macromol. Chem. Phys.* **2010**, *211*, 66−79.
(31) Fornes, T. D.; Paul, D. R. Crystallization behavior of nylon 6 nanocomposites. *Polymer* **2003**, *44*, 3945−3961.
(32) Haggenmueller, R.; Fischer, J. E.; Winey, K. I. Single Wall Carbon Nanotube/Polyethylene Nanocomposites: Nucleating and Templating Polyethylene Crystallites. *Macromolecules* **2006**, *39*, 2964−2971.
(33) Altorbaq, A. S.; Jimenez, A. M.; Pribyl, J.; Benicewicz, B.; Müller, A. J.; Kumar, S. K. Polymer Spherulitic Growth Kinetics Mediated by Nanoparticle Assemblies. *Macromolecules* **2021**, *54*, 1063−1072.
(34) Homminga, D. S.; Goderis, B.; Mathot, V. B. F.; Groeninckx, G. Crystallization behavior of polymer/montmorillonite nanocomposites. Part III. Polyamide-6/montmorillonite nanocomposites, influence of matrix molecular weight, and of montmorillonite type and concentration. *Polymer* **2006**, *47*, 1630−1639.
(35) Fornes, T. D.; Yoon, P. J.; Keskkula, H.; Paul, D. R. Nylon 6 nanocomposites: the effect of matrix molecular weight. *Polymer* **2001**, *42*, 9929−9940.
(36) Krikorian, D. V.; Pochan, J. Unusual Crystallization Behavior of Organoclay Reinforced Poly(l-lactic acid) Nanocomposites. *Macromolecules* **2004**, *37*, 6480−6491.
(37) Ray, S. S.; Bandyopadhyay, J.; Bousmina, M. Influence of degree of intercalation on the crystal growth kinetics of poly-[(butylene succinate)-co-adipate] nanocomposites. *Eur. Polym. J.* **2008**, *44*, 3133−3145.
(38) Avrami, M. Granulation, Phase Change, and Microstructure Kinetics of Phase Change − III. *J. Chem. Phys.* **1941**, *9*, 177.
(39) Mandelkern, L. Crystallization kinetics of homopolymers: Bulk crystallization. In: *Crystallization of Polymers*, Cambridge University Press, Cambridge, 2004. Vol. 2, p. 16−57, and references therein. DOI: 10.1017/CBO9780511535413.
(40) Lorenzo, A. T.; Arnal, M. L.; Albuerne, J.; Müller, A. J. DSC isothermal polymer crystallization kinetics measurements and the use of the Avrami equation to fit the data: Guidelines to avoid common problems. *Polym. Test.* **2007**, *26*, 222−231.
(41) Mandelkern, L. Crystallization kinetics of homopolymers: Bulk crystallization. In: *Crystallization of Polymers*; Cambridge University Press: Cambridge, 2004. Vol. 2, p. 19, and references therein.
(42) Hong, P.-D.; Chung, W.-T.; Hsu, C.-F. Crystallization kinetics and morphology of poly (trimethylene terephthalate). *Polymer* **2002**, *43*, 3335−3343.
(43) Hay, J. N. Secondary crystallization kinetics. *Polym. Crystalliz.* **2018**, *1*, No. e10007.
(44) Moré, J. J. The Levenberg-Marquardt algorithm: Implementation and theory. In: *Numerical Analysis. Lecture Notes in Mathematics*; Watson, G. A. (eds). Springer: Berlin, Heidelberg, 1978, vol. *630*.
(45) Wood, L. A.; Bekkedahl, N. Crystallization of Unvulcanized Rubber at Different Temperatures. *J. Appl. Phys.* **1946**, *17*, 362.
(46) Ergoz, E.; Fatou, J. G.; Mandelkern, L. Molecular Weight Dependence of the Crystallization Kinetics of Linear Polyethylene. I. Experimental Results. *Macromolecules* **1972**, *5*, 147−157.
(47) Magill, J. H. Crystallization kinetics of polytetramethyl-p-silphenylene siloxane (TMPS) fractions. *J. Polym. Sci., Polym. Lett.* **1968**, *6*, 853−857.

https://doi.org/10.1021/acsapm.1c00684
ACS Appl. Polym. Mater. 2021, 3, 5405−5415